Hierarchical biocide-free silicone/graphene-silicon carbide nanocomposite coatings for marine antifouling and superhydrophobicity of ship hulls

Mohammed S. Selim[a], (moh.selim_chem2006@yahoo.com) Ahmed M. Azzam[b,c], (ah.azzam@tbri.gov.eg) Shima A. Higazy[a], (shhigazy@gmail.com) Mohamed A. Shenashen[a,b], (SHENASHEN.Mohameda@nims.go.jp), Ahmed Elmarakbi [d], (ahmed.elmarakbi@northumbria.ac.uk) Mitsuhiro Ebara[b], (EBARA.Mitsuhiro@nims.go.jp) Sherif A. El-Safty[b,*] (sherif.elsafty@nims.go.jp)

[a] Petroleum Application Department, Egyptian Petroleum Research Institute (EPRI), Nasr City 11727, Cairo (Egypt).

[b] Research Center for Macromolecules and Biomaterials, National Institute for Materials Science (NIMS), 1-2-1 Sengen, Tsukubashi, Ibaraki-ken 305-0047, Japan.

[c] Department of Environmental Research, Theodor Bilharz Research Institute (TBRI), P.O. Box 30 -12411, Giza, Egypt.

[d] Faculty of Engineering and Environment, Northumbria University, Newcastle Upon Tyne, NE1 8ST, UK.

E-mail: sherif.elsafty@nims.go.jp; Homepage: https://samurai.nims.go.jp/profiles/sherif_elsafty

Abstract

A new series of fluorine-free, nonbiocidal, and hierarchical superhydrophobic silicone coatings filled with reduced graphene oxide (RGO)/β-SiC bamboo-like nanocomposites was successfully fabricated as durable ternary marine fouling release (FR) surfaces. RGO/β-SiC hybrid was used as coating nanofiller that would release fouling and confer surface robustness. It was facilely created using a straightforward one-phase ultrasonication technique. The dispersion of different concentrations of RGO sheets decorated with β-SiC bamboo-like fillers was determined to study the superhydrophobicity and antifouling behaviors of polysiloxane nanocomposites. RGO was prepared through a simple hydrothermal technique. Solution casting was used to distribute the RGO/β-SiC nanofillers throughout a silicone matrix. Atomic force microscopy, surface free energy, and water contact angle (WCA) were employed to examine the superhydrophobicity and micro/nanoroughness of the coatings. The mechanical, anticorrosive, and durability characteristics of the silicone-RGO/β-SiC-filled composites were also investigated. The antifouling effects of the coating systems were evaluated in the laboratory for 30 days with specific bacteria. The silicone-RGO/β-SiC (3 wt.%) composite with the best dispersion, highest WCA (156°), and lowest surface free energy (12.7 mN/m) among the composites exhibited favorable FR characteristics. The well-dispersed PDMS-RGO/β-SiC (3 wt.% nanofiller) composite presented the minimum degradation and cell viability percentages against Gram-positive and Gram-negative bacteria as well as diatoms. Therefore, this study produced a series of nonstick and fluorine-free ternary FR nanocomposites for maritime coatings with surface durability, superhydrophobicity, and fouling retardancy. This work highlights the design and preparation of multifunctional marine nanocoatings with excellent antifouling performance, easy applicability, and superhydrophobicity properties.

Keywords: *silicone coating, superhydrophobic, fouling release surfaces, micro/nanoroughness, nanofillers, nanocomposite*

1. Introduction

Combating marine fouling is a key strategy and focus area in the field of nanomaterial science for the maritime industry [1]. Biofouling incurs high expenses due to increased fuel consumption, high transportation costs, and hazardous emissions [2,3]. Antifouling paints, which release biocides, were used to stop fouling. These biocides are not only poisonous to marine organisms, they may also impact species that are not their intended targets. Conventional antifouling paints eliminate potential fouling species by leaching biocides [4]. In 2003, the International Maritime Organization issued a global ban on tributyltin-based antifouling paints due to concerns about their detrimental effects on marine life caused by their widespread use [5]. The most common alternatives to tributyltin antifouling surfaces are copper and booster biocide-based coatings. However, they have negative effects on nontarget organisms even at very low concentrations. These materials pose a possible ecological concern to 95% of the organisms in seawater [2,3]. As a result, ecologically friendly alternatives have attracted attention on a global scale [6-8]. Numerous amphiphilic polymers with various macromolecular architectures that are employed in maritime antifouling surfaces have been studied earlier [9,10]. Controlling fouling by using cost- and ecofriendly paint methods is of widespread interest.

Fouling release (FR) coatings have the potential to be used as an environmentally beneficial technology because of their nontoxicity, structural mobility, and low surface free energy (SFE) [11-13]. Fluoropolymers and polysiloxanes, which are components of FR resins, have been shown to perform effectively as fouling-resistant and hydrophobic materials. Fluorinated coatings are commonly designed for the fabrication of superhydrophobic coatings because their smooth surfaces contain $–CF_3$ units and have low surface energy (6.7 mJ/m^2) [14,15]. However, fluorinated compounds may be harmful to the environment as the long-chain perfluorinated alkyl molecules are bioaccumulative and poisonous substances [16,17].

Polysiloxane resins, particularly polydimethylsiloxane (PDMS), are more widely used as a matrix for FR coating functionalities than fluoropolymers [18]. Fluorine atoms are tightly bound in the

fluoropolymer surface, resulting in high stiffness and inhibiting structural rotation along the polymeric backbone. This stiffness also prevents attached biofouling strains from being released easily [19]. Fluorine-free superhydrophobic coatings, such as PDMS, have received considerable attention as ecofriendly surfaces. The water-insoluble matrix PDMS has special qualities as a FR coating. As a result of the presence of two CH_3 groups on each Si atom, PDMS has a low SFE (20 mN/m) [14]. This SFE is lower than the surface energies of polytrifluoroethylene (PTFE, 23.9 mN/m) and polyvinylidene fluoride (PVDF, 30.3 mN/m) [20]. Moreover, PDMS has an exceptionally low elastic modulus of ~1 MPa due to its flexible inorganic –Si–O backbone linkage, which minimizes fouling adhesion on silicone-coated surfaces. The price of PDMS (approximately $6 per kilogram) is considerably lower than that of fluorinated materials, such as PVDF powder ($36.5 per kg) and PTFE emulsion with a solid content of 60% ($30 per kg). PDMS coatings are long-lasting because PMDS has superior wear resistance, toughness, and chemical resistance [21]. Nonstick silicone-based FR surfaces prevent invading species from settling and reduce their adhesion strength without leaching biocidal materials [22].

PDMS fouling prevention depends on suppressing the cohesiveness of submerged structures and inhibiting the fouling settling of such structures through superhydrophobicity action. Consequently, biofilms can be effortlessly removed from surfaces by using straightforward mechanical cleaning or while the vessel is moving [23]. Nevertheless, silicone homopolymers, particularly PDMS, have poor mechanical characteristics and cold flow even at molecular weights of 500,000 g/mol [24,25]. This drawback may be overcome by the addition of nanofillers, particularly those based on graphene, to the polymeric matrix.

Nanomaterials play essential functions in widespread applications from sustainable healthcare to coating industry, affording eco-friendly and comfortable lifestyles [26]. Many nanomaterials, including Cu_2O, TiO_2, Ag, ZnO, carbon nanotubes (CNTs), and reduced graphene oxide (RGO), can be employed as antibacterial agents. The mechanistic antibacterial activity of nanomaterials against microbial cells may be attributed to the massive reactive surfaces of nanoparticles that

interact with cells. This may harm the internal cellular components, cause cell membrane rupture, and deactivate the microbial cells [27,28].

CNTs, graphene oxide (GO), and RGO are some types of carbon allotrope nanoparticles that are utilized to reinforce composites mechanically [29]. They have high tensile strengths and Young's moduli. Due to the interaction of nanofillers with the polymer matrices, the density of these particles strengthens the mechanical properties of nanocomposites [30]. Graphene sheets have closely packed layered structures due to high surface area, vacuum filtration, and intrinsic van der Waals interaction [31]. This may cause agglomeration and prevent the uniform distribution within the polymeric matrix [32]. This agglomeration definitely deteriorates the coating's durability and flexibility. One-dimensional nanomaterials can be used to decorate graphene sheets in order to increase the amount of nanofiller dispersion in the polymeric matrix and inhibit agglomeration. Therefore, a good distribution of graphene-based nanofillers in polymeric matrix could enhance the mechanical properties of nanocomposites [33]. PDMS nanocomposites filled with graphene materials could exhibit outstanding antifouling performance and mechanical robustness [34]. Superhydrophobic nanocomposites are characterized by a ≥150° water contact angle (WCA) and a microscopically rough surface [35,36]. Their surface characteristics are enhanced by atomic-scale surface structures with continuous ribs and grooves oriented along the longitudinal axis [37]. Superhydrophobic coatings with rough surfaces represent original FR surfaces. Graphene has attracted considerable attention worldwide due to its unique chemical and physical characteristics, biocompatibility, electrocatalytic activity, and lack of reactivity to processes [38].

RGO has been employed to design superhydrophobic surfaces because of its hydrophobicity and other characteristics; including high surface area, abrasion resistance, and good antifouling properties [39]. The fabrication of superhydrophobic silicone FR surfaces using graphene/one-dimensional hybrid fillers has been proposed recently [40]. These one-dimensional nanomaterials have vast surface areas and unique shapes that make them particularly appealing for producing rough coatings [41]. Several nanostructured fillers are used to strengthen polymeric materials and

avoid fouling [41]. ZnO nanorod-based coatings could successfully avoid maritime biofouling in static settings [42]. They inhibited bryozoan larvae from forming biofilms and decreased the densities of the marine bacterium *Acinetobacter* AZ4C and the marine alga *Tetraselmis* species. Copper nanowires filled in PDMS resins exhibited long-lasting bacterial resistance and fouling prevention properties [43].

Silicone nanocomposites filled with RGO sheets decorated with β-SiC bamboo-like morphologies have not yet been developed as FR coatings. The modeling of superhydrophobic nanocomposite surfaces employs rough structures with rugged topologies [44]. Chemical vapor deposition, sol–gel, electrospinning, self-assembly, and chemical etching are some of the processes that have been used to create superhydrophobic surfaces [45]. Most of these approaches are challenging and time-consuming, restricting the scope of their industrial applications. In contrast to the above-mentioned methods, solution casting is manageable and economical technique [46]. To the best of our knowledge, no research has been performed on the preparation and application of RGO/β-SiC hybrid composites for filling PDMS FR top coats. The rough topology and low SFE are needed to reproduce water-repellent surfaces based on exfoliated RGO/β-SiC composite arrays. Hierarchical structures introduce outstanding water-repellent properties due to the air trapped between their surface grooves. A global strategic objective is to develop nontoxic and environmental friendly antifouling surfaces with low SFE, superhydrophobicity, and hierarchical roughness for long-lasting ship hull coatings.

Herein, novel nonstick, fluorine-free, and eco-friendly PDMS nanocomposites filled with controlled RGO nanosheet/β-SiC bamboo-like morphologies were developed for the first time as ternary superhydrophobic FR nanosurfaces. Well-distributed nanofillers have the potential to affect the nanocomposite's surface properties. RGO nanosheet/SiC bamboo-like nanofiller was prepared to avoid RGO agglomeration and distribute β-SiC particles on the sheet surfaces. The prepared coatings exhibited superhydrophobicity and mechanical robustness due to their unique micro/nanohierarchical structure with low SFE. The mechanical performance of ternary

nanocoatings was studied. The antifouling performance of the nanocoatings for up to 30 days was analyzed by using a selection of microfoulants, including Gram-negative and Gram-positive bacteria and diatoms. The developed PDMS enriched with RGO/β-SiC (3 wt.%) nanocomposites showed the highest antifouling capabilities against *Escherichia coli* and *Staphylococcus aureus* (Microfouling bacteria) and *Navicula* sp. (Macrofouling diatom). Furthermore, the antibacterial mechanism of the produced superhydrophobic FR nanocoatings was discussed extensively. This study highlighted how the degree of RGO/β-SiC filler dispersion affected silicone nanocoatings' antifouling properties. The created well-dispersed nanocomposite represented the potential to be used as green FR nanocoatings for ship hull coatings.

2. Experimental section

2.1. Chemicals

Graphite flakes with size <20 μm, octamethylcyclotetrasiloxane (D_4, 98%), $NaNO_3$ (99.0%), cesium hydroxide (CsOH, 99.9%), Karstedt catalyst, divinyltetramethyldisiloxane (97%), and polymethylhydrosiloxane were gotten from Sigma–Aldrich, USA. Acros Organics (Belgium) provided $KMnO_4$ (99%), H_2SO_4, (95–97%), orthophosphoric acid (H_3PO_4, 85%), Sodium hydroxide (98%), Ethyl alcohol (99.5%), tetrahydrofuran (THF, 97%), and H_2O_2 (35%). Changsha Sinet Advanced Materials Corporation (China) provided us with pure SiC nanowires (NWs) (99%).

2.2. Fabrication of RGO/β-SiC bamboo-like structures

2.2.1. RGO sheet synthesis

An adapted Hummers method was employed for graphite oxidation to prepare GO nanosheets [47,48]. In a typical process, 72 mL of H_2SO_4 was used to dissolve 0.75 g of powdered graphite and 0.75 g of $NaNO_3$ during continuous stirring. The resulting suspension was added with 4.5 g of $KMnO_4$. Then, the mixture was agitated for 60 min at 35 °C. The temperature was then raised to 90 °C after the mixture was diluted with 60 mL of distilled water. Residual MnO_2 and

permanganate were transformed into Mn(II)SO_4 (colorless) by slowly adding 7.5 mL of H_2O_2. The mixture was filtered with distilled H_2O until its pH reached 7.0. The obtained product was ultrasonicated for exfoliation to yield GO nanosheets, which were centrifuged to remove the unexfoliated solution.

RGO was prepared by the hydrothermal method. This method involved dispersing a specific quantity of nano-GO sheets into distilled H_2O for 20 min under cold conditions followed by 8 h of heating at 200 °C in an autoclave lined with Teflon. After centrifugation, the product was rinsed with a mixture of distilled H_2O and ethanol. Then, the autoclave was allowed to cool naturally overnight. The resultant material was freeze-dried at −50 °C for 24 h to eliminate absorbed solvents and obtain nano-RGO sheets with high homogeneity [49].

2.2.2. Synthesis of RGO/β-SiC bamboo-like nanocomposites

A facile method was used to prepare the RGO/β-SiC nanostructured composite. RGO (50 mg) was ultrasonicated in distilled H_2O (100 mL) for 60 minutes. Then, 50 mL solution of toluene and 50 mg of β-SiC were supplemented with the RGO solution. The produced mixture was continually agitated for 12 hours to make sure that the prepared RGO and β-SiC nanoparticles were completely coordinated. The created composite of the RGO/β-SiC hybrid underwent acetone purification, centrifuged, and purified by washing with THF. The produced RGO/β-SiC hybrid material was homogenized by freeze-drying at -50 °C for 24 h.

2.3. Fabrication of PDMS filled with RGO/β-SiC nanostructured composites:

2.3.1. Unfilled and RGO/β-SiC nanofiller-filled silicone nanocomposites

PDMS resin with vinyl terminals was created through anionic ring-opening polymerization using the D4 monomer and strong base catalyst CsOH [50]. By incorporating various percentages of RGO/β-SiC nanofillers into PDMS resins through the ex-situ technique, a series of PDMS-RGO/β-SiC hybrid composites was created. The obtained virgin and silicone-RGO/β-SiC nanocomposites underwent hydrosilation curing by using the Chalk–Harrods technique [51]. Hydration curing was

conducted on the freshly manufactured virgin PDMS and PDMS-RGO/β-SiC nanocomposites, wherein PMHS interacted with the vinyl terminal chains of the PDMS to form bonds, as follow: Karstedt catalyst (0.1 g) was dissolved in trichloroethylene (30 mL) in a reaction flask with 30 mL of toluene and 13 g of silicone resin to produce solution A. For the preparation of solution B, PMHS (0.3 g) was dissolved in toluene (10 mL) before being progressively supplemented into solution A and vigorously agitated. The mixed solution was degassed for 15 min then coated on several surfaces, allowed to cure overnight, and heated at 70 °C for 3 h.

2.4. Characterization techniques

Several characterization methods were employed to investigate the PDMS-RGO/β-SiC hybrid nanocomposite structure. Gel permeation chromatography (GPC) measurement was carried out by using GPC-1100 Agilent technologies with Waters 2410 refractive index detector styragel columns connected in series using polystyrene as standard and tetrahydrofuran as an eluent. The purity and crystallinity of the RGO/β-SiC nanofiller were characterized by X'Pert PRO XRD (PANalytical diffraction analyzer, UK) using CuK radiation at 2θ of 5°-80°. A Japanese JEOL model JEM2100 LaB6 was used to test HRTEM at 200 kV. Two droplets of the solution were put on the TEM grid after being ultrasonically heated in ethyl alcohol for 10 minutes. A FESEM was employed for studying the topological structure of the surface (JEOL JSM530, Japan). The RGO/β-SiC nanowires hybrid solution was divided into two droplets, ultrasonicated in ethanol, and then put over a glass specimen to dry naturally. The specimens were coated with Au for preventing the charging effects of the electron beam. Moreover, density functional theory (DFT), electrostatic potential, and electron maps (ESP-EM) were used to investigate the hierarchical of RGO/β-SiC hybrid nanofiller according to DMol3 of BIOVIA Dassault systems.

2.5. Surface investigations

The surface hydrophobicity was studied via WCA and SFE determinations. Static WCA of

virgin PDMS and PDMS-RGO/β-SiC nanohybrid materials was assessed using the sessile drop method and Krüss GmbH goniometer (Germany). Total SFE (γ_S^{total}) measurements of unfilled and filled PDMS-RGO/β-SiC nanocomposite were calculated using the geometric-mean method [52]. From this technique, γ_S^{total} represents the sum of polar and dispersive constituents. Using the WCA (θ) results of two different solvents (DI water and diiodomethane), γ_S^{total} was calculated as illustrated in Eqs. (1 and 2) [53]

$$(1 + \cos\theta_L)\gamma_L = 2[\sqrt{\gamma_L^D \gamma_S^D} + \sqrt{\gamma_L^P \gamma_S^P}] \quad (1)$$

$$\gamma_S^{total} = \gamma_S^D + \gamma_S^P \quad (2)$$

θ_L and γ_L are WCA and SFE for the used liquids, respectively. On the other hand, γ_L^D and γ_S^D refer to the surface tension of liquids and surfaces, respectively. A NTEGRA Solaris AFM (Russia) was employed to study the topological structure of the composites. The root mean square roughness (RMS) for the surfaces was calculated using AFM software XEL at 40 N/m force constant, 0.7 Hz scan rate, and 300 kHz resonance frequency.

2.6. Physicomechanical studies

Various mechanical studies such as impact, bend, and crosshatch experiments were employed for assessing coatings' elastic, bendable, and cohesive properties. Virgin silicone and nanocomposite coating tests were done on 17 cm × 9 cm × 0.1 cm dimensions of mild steel specimens. The first coat was an epoxy primer paint with a matrix: hardener mixing ratio 3.7:1 by wt.%. An epoxy/PDMS tie coat with a mixing ratio of 4:1 by wt.% was applied as a second layer. The top layer of the PDMS-RGO/β-SiC nanocomposite had a 150 µm coating thickness. Using an impact Sheen tubular tester (Ref BG5546, UK), the impact tests were carried out following ISO 6272 [54]. The damage resistance of the coated surfaces was assessed by abruptly lowering the impact tester's 1 kg height weight. The substrate-coating adhesion degree was measured using a crosscut tester (Sheen SH 750, UK) that had 6-teeth of 1.5 mm steel cutter. The cross-cut region

was covered with pressure tape, flattened, and pulled before applying ASTM D 3359 to gauge the adhesion level [55]. The nanocomposite coatings' elasticity was evaluated by mandrel bend experiment [56]. The mandrel diameter of the Ref. 809 model Sheen bend tester (UK) was between 3.2 and 38 mm.

2.7. Antifouling assessments

2.7.1. Diatom and bacterial growth inhibition

Fouling-related performance can be assessed by using diatoms and different bacterial species that form biofilms on different surfaces [57]. Diatoms were used to study the antifouling performance of the designed coatings [58]. The FR activity of the RGO/β-SiC nanostructured composite was determined by using *Navicula* sp. diatoms [59]. The diatoms were collected and purified from Qarun Lake, Fayoum Governorate, Egypt. In natural saltwater and F/2 medium, diatom cultures were grown to a density of 10^3 cells/mL and then incubated for 72 hours at 26 °C. In this work, cultures with different concentrations were prepared from stock culture by using sterile F/2 culture medium. A total of 10 mL of *Navicula* sp. was suspended in F/2 medium (OD_{660} nm = 0.015), placed in Petri dishes, then coated onto slides with various concentrations (0.25%, 0.5%, 1%, 2%, and 3%) of nanostructure fillers submerged in the dishes (triplicate). Slides coated with 0.0% nanofillers were used as a control. Then, the cells were incubated at RT (25 °C) for 4 weeks. After incubation, the slides were removed and washed. Subsequently, the attached diatom cells were counted (mean ± SD) under a microscope. *E. coli* and *S. aureus*, which are frequently found in biofilms and isolated from water, were used to test the resistance of the unfilled and filled nanocoatings to bacterial growth in water and the bacterial density after exposure to the coated surface. A Luria broth medium culture test was used to examine the antimicrobial effectiveness of the coated and uncoated slides against *E. coli* and *S. aureus* [60]. This assessment could indicate whether microbial growth was inhibited at a particular time by measuring an end point. The Luria broth (Sigma Aldrich, UK) was utilized to grow *E. coli* and *S. aureus* bacterial stock cultures for 24

h at 30 °C. The bacterial cultures were diluted to an initial density of 10^6 cells/mL after incubation in broth media. Each slide (25 mm × 75 mm) was coated with PDMS-RGO/β-SiC nanocomposites and placed in a sterile flask containing bacterial cultures (100 mL). At 1, 2, and 4 weeks, the test was performed three times on a shaker (20 rpm) at 30 °C. Following incubation, the culture's optical densities at 600 nm for the nanocomposite samples were assessed and compared with those of the control treatments.

2.7.2. Mesocosm study

The ability of biofouling bacteria to adhere to coated slide surfaces was examined. Empty and loaded nanostructure slides were submerged in three aquarium groups containing sterile surface water. Three slides coated with 3% silicone/graphene–SiC hierarchical nanostructures, along with three uncoated glass specimens as control specimens, were included in each tank group. Samples were taken after 1, 2, and 4 weeks. The coated samples were incubated at 25 °C. One coated specimen was removed from each container after treatment. The biofilm that had adhered to the slides was removed by using a sterile scalpel [61,62]. The biofilm samples were fixed with 3% paraformaldehyde in phosphate-buffered saline (1:1). A portion of the resultant biofilm suspension was stained by using SYTO 9 green fluorescent nucleic acid (Life Technologies, Thermo Fisher, United States) to allow the observation of living microbial cells. A Zeiss Leica Microsystems Imaging Solution (Germany) inverted epifluorescence or reflectance laser scanning confocal microscope with a magnification power of 1000× was used for microscopy. The specimens were held in the dark for 20 min before examination. The formation of bacterial biofilm growth on the coated glass slides of the modeled PDMS-RGO/β-SiC was recorded after incubation for comparison with that on the untreated slides. After dilution, flow cytometry was used to count the number of live cells in the biofilm suspension samples after labeling with SYBR green for 15 min in the dark (FACSCanto II cytometer).

3. Results & discussion

3.1. Controlled fabrication and structure of hierarchical RGO/β-SiC nanofillers

Vinyl-terminated PDMS nanocomposites filled with RGO sheet/β-SiC bamboo-like hybrids were prepared via solution casting for applying as durable marine FR coatings. A facile one-phase ultrasonication technique was used to prepare RGO/β-SiC hybrid nanofillers as antifoulant materials. Figure 1 compared the XRD spectra of the produced materials. The d-spacing of the main peak observed at 2Θ=10.3° (for the GO [002] crystal facet) was 0.95 nm, which was larger than that of natural graphite (0.34 nm). The enhancement in interlayer distance might be due to the production of oxygen on the nano-GO surface [63]. In the XRD spectra of SiC nanowires (NWs), the peaks at 35.7°, 41.3°, 60.05°, 71.1°, and 75.5° seen at 2 h were due to the (111), (200), (220) and (311), and (222) crystal orientations, respectively. The splitting factor was caused by inaccurate stacking for the peak recorded at 33.77° [64]. The results showed that SiC NWs with dominant (111) facets, which were indicative of the maximum intensity, had high surface crystallinity and purity. The average diameter estimated by using the Debye–Scherrer equation was 55 nm. The RGO diffraction peaks in the XRD pattern of the RGO/β-SiC nanocomposite revealed that the RGO nanosheets had been decorated with β-SiC nanowires. It indicated that SiC NWs anchored on the RGO sheets through the (111) crystal plane. This is attributed to the fact that (111) crystal planes in SiC NWs have lower surface energy, and the construction process of the jointing sites may tend to proceed along the lowest energy plane [65,66].

In the RGO/β-SiC hybrids, the diffraction peak dramatically decreased to 9.6, indicating that exfoliation had sufficiently loosened and disorganized RGO sheets [67]. However, the anchoring technique did not affect the structural integrity of the RGO sheets (Scheme 1).

FETEM was able to capture the sizes and morphologies of the as-synthesized nanomaterials (Figure 2). Figure 2 (A and B) depicted that the GO sheets had folded edge structures and wrinkled forms. Such nanosheets might function as nanoblades that could rip through cell membranes because of their thin edges, which had thicknesses of 0.5–2 nm. HRTEM (Figure 2 (C and D))

revealed that the SiC nanomaterial had a consistent NW structure with an average diameter of 50–80 nm and average length of 1–2 mm. The HRTEM images in Figure 2 (G and H) demonstrated that the RGO/β-SiC hybrid nanocomposites featured wrinkled edges on the surfaces of the GO nanosheets, which were enriched with SiC wires. These images depicted the good dispersion of the SiC NWs on the surfaces of the GO nanosheets. Well-dispersion of β-SiC NWs throughout the RGO nanosheets demonstrated the successful fabrication of the RGO/β-SiC nanocomposites via a facile one-phase ultrasonication method.

Figure 3 displayed a FESEM image of the shape and structure of the created nanostructures. The layered structure and wrinkled edges of the GO nanosheets were shown in Figure 3 (A and B). The wrinkled edges of the GO nanosheets reflected the exfoliation of graphite throughout oxidation. Figure 3 (C and D) show that β-SiC NWs had an NW shape with a mean diameter of 60 nm. The composite of RGO/β-SiC NWs was shown in Figure 3 (E and F), wherein β-SiC NWs were evenly distributed on the RGO surface. This resulted in the formation of a pure and reliable hybrid nanocomposite. The results confirmed that RGO sheets were successfully decorated with β-SiC NWs to produce pure RGO/β-SiC hybrid nanofillers. SiC NWs were absorbed on the surface of RGO due to the hydrogen bonding between the hydroxyl group of SiC NWs and the residual oxygen-containing groups of RGO [68-70]. Therefore, RGO could connect with SiC NWs in PDMS matrix, promoting the formation of filler network. The controlled size and morphological structure of the nanofillers played a prominent role in enhancing surface durability, reducing SFE, micro/nano hierarchical roughness, water repellency; and antifouling performance.

3.2. Ex-situ methodological approach for the fabrication of hybrid PDMS-RGO/β-SiC nanocomposites

Given the promising features of vinyl-ended PDMS in FR self-cleaning paints, high molecular weight (MW) vinyl-ended PDMS nanosurfaces were prepared. Alkali metal solubility and reactivity increased with increasing size of cation during D4 polymerization [71,72]. CsOH dissolved below

100 °C, KOH dissolved at ~150 °C, and NaOH and LiOH were not dissolved even above 150 °C. The reactivity of CsOH was > RbOH > KOH > NaOH > LiOH [72]. Moisture-free catalyst is crucial to yield high MW polymer. The molar concentration ratio of D4 to the end capping reagent and catalyst type are major factors for MW control. Increased MW of PDMS improves the mechanical properties as compared with the low MW analogs [73]. GPC measurements reflected the high MW of the prepared PDMS, where the MW and polydispersity values were 232537 g/mol and 1.51, respectively (Supplementary material, Fig. S1). The vinyl content of the prepared PDMS was determined by iodometric titration method and the result was 2.9 ± 0.2 mol% (Supplementary material).

The RGO/β-SiC hybrid was mixed at various concentrations with PDMS matrix to increase surface inactivity and inhibit fouling adhesion. This method aimed to determine the appropriate degree of fouling repellency. SEM was employed to analyze nanofiller dispersion and homogeneity in the PDMS resin. The dispersion of the nanofillers into the PDMS resin was evaluated by using FESEM (Figure 4 (A–C)). The FESEM scan showed that the bare PDMS coating had a featureless and smooth surface (Figure 4A). Roughness increased with high loadings of RGO/β-SiC NW (1 wt.%) in the PDMS resin (Figure 4B). The PDMS nanocomposite filled with well-dispersed RGO/β-SiC NW (3 wt.%) nanofillers exhibited high surface roughness and enabled FR performance (Figure 4C). The insertion of RGO/β-SiC nanofillers into the channels of the polymer nanocomposite results in the formation of a hydrogen bonding interaction that restricted polymer chain mobility. The high surface roughness of the PDMS-RGO/β-SiC nanocomposite could be attributed to the following reasons: (1) the synergistic effect of RGO and SiC NWs in the formation of filler network; (2) the macroscopically and microcosmically orderly filler network; (3) the decrease of interfacial defects due to the formation of well-dispersed PDMS-RGO/β-SiC nanocomposite; (4) The rise in the solid-liquid interface might increase surface roughness and hydrophobicity by trapping air in the surface grooves to produce superhydrophobic surfaces. The resulting nanocomposites may have improved interfacial bonding due to extra-high surface-area,

and matrix-nanofiller interfacial bonding.

The micro/nano-particles are usually used to generate coating surface roughness. According to Wang et al. [14], assembling particles of various sizes can improve surface roughness and superhydrophobicity. Cortese et al. [74] used PDMS microstructuring to create a variety of structures with mono and dual hierarchical roughness by merely replicating pre-patterned structures using a CF4 plasma treatment. The fabricated superhydrophobic PDMS surface exhibited WCA up to 170°. According to Barthwal et al. [75], a composite of PDMS-modified multiwall CNTs (MWCNTs)/ZnO (2.5 wt.% nanofiller) showed a microrough superhydrophobic surface with 156° WCA for anti-fouling and anticorrosion applications. Well-dispersed PDMS-RGO/β-SiC (3 wt.%) rough surface with tailored micro/nano-textures can improve the stability of superhydrophobicity by decreasing the convexity of the liquid/air interface and maintaining the contact angle away from its critical advancing value [76].

By contrast, higher nanofillers (4 and 5 wt.%) showed a reduction in the topological homogeneity and roughness because of the fillers' agglomeration. This caused heterogeneous rough structure, enabled sliding the drops of water inside the grooves results in wettability and lower hydrophobic and antifouling performance. Nanofillers' well-dispersion is necessary to avoid agglomerations, cracking, and brittleness caused at higher nanofillers concentrations.

3.3. Theoretical and experimental studies on the surface functionality of nanocoating composites

The nonwettability properties, surface topology, functionality, and activity of the nanocoating composites were investigated on the basis of density function theory (DFT) calculations, electrostatic potential charges, and surface microscopy (Figures (4 and 5)). Nanoscale topography significantly contributed to the creation of a surface with wettability that nearly resembles the wettability of naturally rough surfaces. In addition, as shown in Figure 4, surface topology was studied to understand the hydrophobic or hydrophilic surface features involved in coating applications. Atomic force microscopy was conducted to reveal the surface topology and roughness

of the coated nanofiller structure as illustrated in Figure 4 (D–F). The unfilled coating exhibited a featureless surface with an RMS value of 0.94 nm (Figure 4D). Silicone specimens that were filled with 1 wt.% RGO/β-SiC had highly pronounced surface roughness and FR effects (13.18 nm) (Figure 4E). Among the coatings, the PDMS-RGO/β-SiC (3 wt.%) coating had the topology with the highest RMS (79.18 nm) because of its good nanofiller distribution and high WCA (Figure 4F). DFT analysis was performed to determine electrostatic (+ve or −ve range) isosurface potential and electron maps of the composite surfaces for identifying the influence of hierarchal geometry and surface roughness. They exhibited important roles in determining surface orientation, morphology, electron/charge potential, and electron mobility during the superhydrophobicity of the nanocoatings (Figure 5). Indeed, the self-assembly of the nanosheet discs in a longitudinal bamboo-like orientation and within the RGO/β-SiC hybrid nanocomposites might create widespread surface electron/charge diffusion, leading to high electron mobility during superhydrophobicity (Figure 5A). Additionally, DFT analysis was used to explore the retention of 3D modeling structure projections along the hierarchical RGO/β-SiC hybrid nanocomposite architecture. The hybrid RGO/β-SiC nanocomposites presented a hierarchical structure due to strong electrostatic attraction and lamellar stacking. This structure improved the superhydrophobicity and antifouling performances of the nanocomposites. The β-SiC hybrid nanocomposites preserved their configuration planes and crystal-structure surfaces (Figure 5). The crystal-building structures of the composites with a hierarchical architecture (Figure 5A) presented cages, grooves, and holes along the hierarchical apex and edges for efficiently achieving high-mobility charge flows and transitions during the nanocomposites' superhydrophobicity. Figure 5B showed the surface charge configuration and electrostatic electron mobility along a wide range of domains shown by the composite film surfaces. The electronic and charge map configuration indicated the potential effect of the vast transport, high mobility, and electrons/charges' flow along the nanocomposite surfaces on the superhydrophobicity and antifouling performance (Figures 6–8).

Figure 6 showed that WCA was performed to investigate the superhydrophobicity of the modeled

coatings before and after they were submerged for 7 days in distilled water. A sample of a virgin PDMS coating showed hydrophobic properties with a WCA of 106°. The nonwettability of the PDMS-RGO/β-SiC composites significantly increased with increasing RGO/β-SiC nanofiller concentrations. The WCA increased to 156° with the addition of 3 wt.% nanofillers. The findings showed that a good nanofiller distribution could result in surface superhydrophobicity because of coating–nanofiller interfacial forces, high surface areas, and improved roughness. The WCA was reduced to 136° and 122° with the addition of higher concentrations (4 and 5 wt.% nanofillers, respectively). Increasing the RGO/β-SiC nanofiller percentages up to 4 and 5 wt.%, reduced the water repellency owing the nanofillers agglomerations. This could destroy the matrix–nanofillers interfacial bonds and strengthened the agglomeration linkages, where the surface areas of nanofillers were reduced. The submerged samples had lower WCAs than the initial samples (Figure 6), proving that the PDMS-RGO/β-SiC nanocomposites had regenerative properties. The findings indicated that the total SFE was constantly decreased from 21.46 for the virgin PDMS to 12.4 mN/m with the addition of 3 wt.% RGO/β-SiC nanofillers. The surface topology was roughened, which decreased adhesion to the fouling bonds. The minimum SFE and greatest roughness were obtained by adding evenly dispersed RGO/β-SiC (3 wt.%) fillers into the silicone resin, which prevented fouling adhesion. By reducing SFE and promoting air entrapment in the surface grooves, this slick architecture encouraged superhydrophobicity and demonstrated the advantages of a water-repellent FR coating.

The densely packed PDMS-RGO/β-SiC nanocomposite layer enhanced the surface roughness, according to Cassie–Baxter mode. This may trap air in the surface interstices and inhibit water droplets from sliding inside these interstices' groves. This rough surface is equivalent to a composite surface of solid and air pockets and is correlated with the surface chemical heterogeneity and roughness. Because air is a superhydrophobic characteristic with a WCA of 180°, the rough surface amplifies superhydrophobicity [77]. Surface roughness is well-known as a key element in achieving superhydrophobicity [78]. The PDMS-RGO/β-SiC (3 wt.%) rough surface with optimized micro-

textures can prevent the Cassie-Baxter mode from switching to the Wenzel mode. As a result, the liquid/air interface becomes less convex and the contact angle remains away from its critical advancing value, improving the stability of superhydrophobicity and FR performance [76].

By contrast, the total SFE was increased by the addition of higher RGO/β-SiC nanofillers loadings (15.53 mN/m for 4 wt.% and 17.2 for 5 wt.%), respectively. This was caused by the nanofillers' agglomerations, lower surface-area, minimized the PDMS-nanofillers interfacial bonding, and increased particle clustering.

3.4. Coating durability of PDMS-RGO/β-SiC nanocomposites

It was necessary to investigate the flexibility and adhesion properties of the developed PDMS-RGO/β-SiC nanocomposites for applying as surface coatings [79]. The nanocomposites created with various nanofiller concentrations were investigated through impact, crosscut, and T-bending experiments. In the impact experiment on the developed PDMS-RGO/β-SiC coating, no cracks up to 16 Joule were seen, demonstrating the coating's high flexibility and durability (Table 1). The high impact resistance was induced by the silicone's interlayer high free volume and the mechanical durability produced via the homogeneity of the dispersion of RGO/β-SiC nanofillers in the matrix. Additionally, no cohesion flaws were found during the crosscut experiment (Table 1). After being subjected to mandrel bending over a tubular spindle of 5 mm, the samples exhibited no apparent incursions or cracks visually or under microscopy (Table 1). These findings demonstrated the high mechanical durability of the distributed PDMS-RGO/β-SiC nanocomposites. The improved adherence and flexibility of the coating to the substrate are the outcome of the PDMS matrix's good interactions with RGO/β-SiC nanofillers. Well-dispersed RGO/β-SiC nanofillers formed a cross-linked network and a strong interfacial interaction with PDMS surface, which can be concluded as the critical factor for surface durability. Physical networks eventually resulted from chemisorption and/or physisorption. These results demonstrated the importance of the homogenous dispersion of PDMS-RGO/β-SiC nanocomposites for high mechanical robustness. The well-dispersed

nanocoatings' high flexibility and adherence to the substrate demonstrated their long-term robustness.

3.5. Antifouling efficacy of PDMS-RGO/β-SiC nanocomposites

The water microfouling bacteria (*E. coli* and *S. aureus*) and the macrofouling diatom (*Navicula* sp.) were used as predominant maritime biofilm formers that could resist many antifouling coatings. The growth of these strains was significantly inhibited by the PDMS-RGO/β-SiC hierarchical nanostructure coatings. Compared with the virgin PDMS control samples, the hierarchical nanostructure coating reduced the density of diatoms by 69%. The PDMS-RGO/β-SiC nanostructured composite coatings almost completely inhibited (97%) diatom growth (Figure 7). The addition of up to 3% hierarchical nanostructures enhanced the antibacterial activity of the PDMS-RGO/β-SiC nanocomposite coating against *S. aureus* and *E. coli*. This resulted in the strongest antibacterial effect as reflected in the reduction in bacterial count (Figure 8A).

After incubation time for 4 weeks, the remaining viable bacterial counts were only 11% for PDMS-RGO/β-SiC (3 wt.% nanofillers) as compared to virgin PDMS (Figure 8B). This finding reported the high antibacterial performance of the well-dispersed PDMS-RGO/β-SiC nanocomposite, caused by the increased nanocoating's interfacial bonding and WCA yielding outstanding FR surface. The surface roughness and superhydrophobicity significantly reduce the number of adherent bacteria with enhanced fouling-antiadhesion [80]. In addition, SEM images (Figure 9) showed that the adherence of bacterial cells to the prepared surfaces decreased with increasing nanofiller percentages. Similarly, numerous investigations have demonstrated that hierarchical nanostructures have antimicrobial activities against a variety of bacterial species [7].

For the investigation of cell viability, fluorescence microscopy was used to examine further the biofilm suspension that accumulated from the virgin and filled hierarchical nanostructure samples after 4 weeks of incubation (Figure 10). Compared with those of the virgin PDMS and control samples, the biofilm specimens of the PDMS-RGO/β-SiC nanocomposites exhibited a noticeably

lower number of viable cells. Most of the cells on the control samples were alive and grouped together. By contrast, only few cells were visible in the biofilms on the nanostructure coatings. Well-dispersed hierarchical RGO/β-SiC nanofillers could exhibit high antifouling behavior. The number of cells significantly decreased with RGO/β-SiC nanofillers' insertion up to 3 wt.%. These findings supported the inhibiting effect of hierarchical nanostructures and were consistent with the results of contact angle and SFE measurements. The inclusion of hierarchical nanostructures into a silicone antifouling surface was an efficient technique for preventing microbial growth on submerged coatings on the basis of surface superhydrophobicity. The distribution of RGO/β-SiC nanofillers (3 wt.%) resulted in the substantial growth inhibition of microorganisms. Various fouling organisms were prevented from adhering to the developed nontoxic and nonleaching silicone nanocomposites via a fouling-repellency mechanism. This outcome was achieved through the development of micro/nano-rough topologies, reduction in SFE, and nonwettable FR coatings. Surface FR performance was produced by reducing SFE and increasing WCA. Thus, the good dispersion of 3 wt.% RGO/β-SiC hybrid fillers in PDMS resin provided outstanding antifouling performance and mechanical durability. The PDMS–nanofiller interfacial bonding and coating–substrate cohesion forces were increased by the superior dispersion of the fillers. The rough topology could enhance the surface superhydrophobicity and prevent water from entering the surface grooves of interstices [81]. A physical anticohesion mechanism prevented diverse bacterial and diatom species from adhering to the developed nontoxic PDMS-derived nanocomposites. Therefore, the novel coating nanocomposites showed high antifouling activity against the tested macro- and microorganisms, making them very suitable for use in the maritime shipping industry.

4. Conclusions

For the first time, an ecofriendly, nonstick, and superhydrophobic series of PDMS-RGO/β-SiC nanocomposites was developed as robust marine FR coatings for ship hulls. A facile method was used to prepare RGO/β-SiC nanofillers for using as advanced antifoulant nanoagents. For

comparison, different percentages of RGO/β-SiC nanofillers were dispersed into a silicone matrix. Bamboo-like SiC nanoparticles had a definite morphology, [111] orientation, and an average width of 80 nm. The superhydrophobicity, mechanical toughness, and antifouling properties of the developed coatings were thoroughly investigated. Selected Gram-positive and Gram-negative bacteria as well as diatoms were evaluated by many antifouling assays to assess the FR efficacy of the nanocomposites. The well-distributed PDMS-RGO/β-SiC composite with 3 wt% nanofiller showed the lowest SFE, highest WCA (156°), roughest topology (micro/nanoscale), and outstanding FR features. The developed nanocoating offered high mechanical durability. Cell viability as well as scanning electron and fluorescence microscopy results demonstrated that the well-dispersed nanocoatings presented high resistance against various bacteria and diatoms by exerting surface superhydrophobicity. Overall, our research showed that the created nanocomposite coatings were economical, long-lasting, and ecofriendly antifouling surfaces for maritime navigation.

Acknowledgement

This work was supported by the Egyptian Petroleum Research Institute (EPRI in Egypt), Center for Functional Materials, National Institute for Materials Science (NIMS in Japan), and Nano-Environmental Uint (NEU), Theodor Bilharz Research Institute (TBRI in Egypt).

Conflicts of Interest:

The authors declare no conflict of interest.

References

[1] S. Pourhashem, A. Seif, F. Saba, E.G. Nezhad, X. Ji, Z. Zhou, X. Zhai, M. Mirzaee, J. Duan, A. Rashidi, B. Hou, Antifouling nanocomposite polymer coatings for marine applications: A review on experiments, mechanisms, and theoretical studies, J. Mater. Sci. Technol. 118 (2022) 73-113.

[2] M.S. Selim, S.A. El-Safty, M.A. Shenashen, S.A. Higazy, A. Elmarakbi, Progress in biomimetic

leverages for marine antifouling using nanocomposite coatings, J. Mater. Chem. B 8 (2020) 3701-3732.

[3] M.S. Selim, M.A. Shenashen, S.A. El-Safty, M. Sakai, S.A. Higazy, H. Isago, A. Elmarakbi. Recent progress in marine foul-release polymeric nanocomposite coatings. Prog. Mater. Sci. 87 (2017) 1-3.

[4] L. Chen, Y. Duan, M. Cui, R. Huang, R. Su, W. Qi, Z. He, Biomimetic surface coatings for marine antifouling: Natural antifoulants, synthetic polymers and surface microtopography, Sci. Total Environ. 766 (2021) 144469.

[5] D.D. de Oliveira, E.G. Rojas, M.A.S. Fernandez, Should TBT continue to be considered an issue in dredging port areas? A brief review of the global evidence, Ocean Coastal Manag. 197 (2020) 105303.

[6] H. Jin, L. Tian, W. Bing, J. Zhao, L. Ren, Bioinspired marine antifouling coatings: Status, prospects, and future, Prog. Mater. Sci. 124 (2022) 100889.

[7] R.B. Bodkhe, S.J. Stafslien, J. Daniels, N. Cilz, A.J. Muelhberg, S.E.M. Thompson, M.E. Callow, J.A. Callow, D.C. Webster, Zwitterionic siloxane-polyurethane fouling-release coatings, Prog. Org. Coat. 78 (2015) 369-380.

[8] H. Thérien-Aubin, L. Chen, C.K. Ober, Fouling-resistant polymer brush coatings, Polymer 52 (24) (2011) 5419-5425.

[9] G. Galli, E. Martinelli, Amphiphilic Polymer Platforms: Surface Engineering of Films for Marine Antibiofouling, Macromol. Rapid Commun. 38 (8) (2017) 1600704.

[10] R.W. van Zoelen, H. Buss, N.C. Ellebracht, N. Lynd, D. Fischer, J. Finlay, S. Hill, M.E. Callow, J.A. Callow, E. Kramer, R.N. Zuckermann, R.A. Segalman, Sequence of hydrophobic and hydrophilic residues in amphiphilic polymer coatings affects surface structure and marine antifouling/fouling release properties, Macro Lett. 3 (4) (2014) 364-368.

[11] A.K. Leonardi, R. Medhi, A. Zhang, N. Düzen, J.A. Finlay, J.L. Clarke, A.S. Clare, C.K. Ober, Investigation of N-substituted morpholine structures in an amphiphilic PDMS-based antifouling and

fouling-release coating, Biomacromolecules, 23 (6) (2022) 2697-2712.

[12] A.K. Leonardi, C.K. Ober, Polymer-based marine antifouling and fouling release surfaces: strategies for synthesis and modification, Annu. Rev. Chem. Biomol. Eng. 10 (2019) 241–264.

[13] A. Leonardi, A.C. Zhang, N. Düzen, N. Aldred, J.A. Finlay, J.L. Clarke, A.S. Clare, R.A. Segalman, C.K. Ober, Amphiphilic nitroxide-bearing siloxane-based block copolymer coatings for enhanced marine fouling release, ACS Appl. Mater. Interfaces, 13 (24) (2021) 28790-28801.

[14] Q. Wang, G. Sun, Q. Tong, W. Yang, W. Hao, Fluorine-free superhydrophobic coatings from polydimethylsiloxane for sustainable chemical engineering: Preparation methods and applications, Chem. Engin. J. 426 (2021) 130829.

[15] S. Krishnan, N. Wang, C.K. Ober, J.A. Finlay, M.E. Callow, J.A. Callow, A. Hexemer, K.E. Sohn, E.J. Kramer, D.A. Fischer, Comparison of the fouling release properties of hydrophobic fluorinated and hydrophilic PEGylated block copolymer surfaces: Attachment strength of the diatom *Navicula* and the green alga *Ulva*, Biomacromol. 7 (5) (2006) 1449-1462.

[16] M. Scheringer, X. Trier, I.T. Cousins, P. de Voogt, T. Fletcher, Z. Wang, T.F. Webster, Helsingør Statement on poly- and perfluorinated alkyl substances [PFASs], Chemosphere 114 (2014) 337-339.

[17] E. Gorrochategui, E. Pérez-Albaladejo, J. Casas, S. Lacorte, C. Porte, Perfluorinated chemicals: Differential toxicity, inhibition of aromatase activity and alteration of cellular lipids in human placental cells, Toxicol. Appl. Pharmacol. 277 (2014) 124-130.

[18] P. Hu, Q. Xie, C. Ma, G. Zhang, Silicone-based fouling-release coatings for marine antifouling, Langmuir 36 (9) (2020) 2170–2183.

[19] A.M.C. Maan, A.H. Hofman, W.M. de Vos, M. Kamperman, Recent developments and practical feasibility of polymer-based antifouling coatings, Adv. Funct. Mater. 30 (32) (2020) 2000936.

[20] H. Peng, Synthesis, Application of fluorine-containing polymers with low surface energy, Polym. Rev. 4 (2019) 739-757.

[21] X. Zhu, X. He, X. Cui, G. Zhu, Y. Pan, Q. Shao, C. Zhao, M. Dong, Y. Zhang, Z. Guo, Polydimethylsiloxane-titania nanocomposite coating: Fabrication and corrosion resistance, Polymer 138 (2018) 203-210.

[22] T.P. Galhenage, D. Hoffman, S.D. Silbert, S.J. Stafslien, J. Daniels, T. Miljkovic, J.A. Finlay, S.C. Franco, A.S. Clare, B.T. Nedved, M.G. Hadfield, D.E. Wendt, G. Waltz, L. Brewer, S.L.M. Teo, C-S. Lim, D.C. Webster, Fouling-release performance of silicone oil-modified siloxane-polyurethane coatings, ACS Appl. Mater. Interfaces 8 (42) (2016) 29025-29036.

[23] (a) Y. Lin, Y. Xie, F. Chen, S. Gong, W. Yang, X. Liang, Y. Lian, J. Chen, F. Wei, W. Bai, Y. Xu, R. Jian, Bioinspired self-stratification fouling release silicone coating with strong adhesion to substrate, Chem. Engin. J. 466 (part 2) (2022) 137043; (b) E. Yilgor and I. Yilgor, Silicone containing copolymers: Synthesis, properties and applications, Prog. Polym. Sci. 39 (2014) 1165-1195.

[24] M.S. Selim, S.A. El-Safty, M.A. Shenashen, Chapter 8 - Superhydrophobic foul resistant and self-cleaning polymer coating, In: Superhydrophobic Polymer Coatings, (Eds. S.K. Samal, S. Mohanty, S.K. Nayak,) (Elsevier Scientific Publisher Company, New York, 2019, 181-203).

[25] A. Rahimi, S.J. Stafslien, L. Vanderwal, J.A. Finlay, A.S. Clare, D.C. Webster, Amphiphilic zwitterionic-PDMS-based surface-modifying additives to tune fouling-release of siloxane-polyurethane marine coatings, Prog. Org. Coat. 149 (2020) 105931.

[26] M.S. Selim, A.M. Azzam, M.A. Shenashen, S.A. Higazy, B.B. Mostafa, S.A. El-Safty, Comparative study between three carbonaceous nanoblades and nanodarts for antimicrobial applications, J. Environ. Sci. 136 (2024) 594-605.

[27] A.M. Azzam, M.A. Shenashen, A.Tawfik, N.A. Safwat, B.B. Mostafa, S.A. El-Safty. Antimicrobial activity of mesoporous organic functionalized hexagon Fe_3O_4 nanosheets for wastewater treatment, Environ. Nanotechnol. Monit. Manag. 18 (2022) 100739.

[28] A.M. Azzam, M.A. Shenashen, M.S. Selim, B. Mostafa, A., Tawfik, S.A. El-Safty, Vancomycin-loaded furriness amino magnetic nanospheres for rapid detection of gram-positive

water bacterial contamination, Nanomater. 12 (2022) 510.

[29] C.I. Idumah, Novel advancements in green and sustainable polymeric nanocomposites coatings, Curr. Res. Green Sustain. Chem. 4 (2021) 100173,

[30] A. Beigbeder, R. Mincheva, M.E. Pettitt, M.E. Callow, J.A. Callow, M. Claes, P. Dubois, Marine fouling release silicone/carbon nanotube nanocomposite coatings: on the importance of the nanotube dispersion state, J. Nanosci. Nanotechnol. 10 (2010) 2972–2978.

[31] M.J. McAllister, J.-L. Li, D.H. Adamson, H.C. Schniepp, A.A. Abdala, J. Liu, M. Herrera-Alonso, D.L. Milius, R. Car, R.K. Prud'homme, I.A. Aksay, Single sheet functionalized graphene by oxidation and thermal expansion of graphite, Chem. Mater. 19 (2007) 4396.

[32] S. Stankovich, D.A. Dikin, R.D. Piner, K.A. Kohlhaas, A. Kleinhammes, Y. Jia, Y. Wu, S.T. Nguyen, R.S. Ruoff, Synthesis of graphene-based nanosheets via chemical reduction of exfoliated graphite oxide, Carbon 45 (2007) 1558–1565.

[33] L. Cavas, P.G. Yildiz, P. Mimigianni, A. Sapalidis, S. Nitodas, Reinforcement effects of multiwall carbon nanotubes and graphene oxide on PDMS marine coatings, J. Coat. Technol. Res. 15 (2018) 105–120.

[34] S. Soleimani, A. Jannesari, M. Yousefzadi, A. Ghaderi, A. Shahdadi, Eco-friendly foul release coatings based on a novel reduced graphene oxide/Ag nanocomposite prepared by a green synthesis approach, Prog. Org. Coat. 151 (2021) 106107.

[35] P. Nguyen-Tri, H.N. Tran, C.O. Plamondon, L. Tuduri, D-V. N. Vo, S. Nanda, A. Mishra, H-P. Chao, A.K. Bajpai, Recent progress in the preparation, properties and applications of superhydrophobic nano based coatings and surfaces: A review, Prog. Org. Coat. 132 (2019) 235-256.

[36] Y. Lin, Y. Xie, F. Chen, S. Gong, W. Yang, X. Liang, Y. Lian, J. Chen, F. Wei, W. Bai, Y. Xu, R. Jian, Bioinspired self-stratification fouling release silicone coating with strong adhesion to substrate, Chem. Engin. J. 446, Part 2 (2022) 137043.

[37] D. Hassen, S.A. El-Safty, K. Tsuchiya, A. Chatterjee, A. Elmarakbi, M.A. Shenashen, M.

Sakai, Longitudinal hierarchy Co_3O_4 mesocrystals with high-dense exposure facets and anisotropic interfaces for direct-ethanol fuel cells, Sci. Rep. 6 (2016) 24330.

[38] A. Elbourne, R.J. Crawford, E.P. Ivanova, Nano-structured antimicrobial surfaces: From nature to synthetic analogues, J. Colloid Interface Sci. 508 (2017) 603-616.

[39] Z. Bai, B. Zhang, Fabrication of superhydrophobic reduced-graphene oxide/nickel coating with mechanical durability, self-cleaning and anticorrosion performance, Nano Mater. Sci. 2(2) (2020) 151-158.

[40] S. Yu, Y. Yang, L. Ma, W. Jia, Q. Zhou, J. Zhu, J. Wang, SiC nanowires enhanced graphene composite coatings with excellent tribological and anticorrosive properties, Tribol. Inter. 188 (2023) 108894.

[41] D. Liu, A. Wang, G. Wang, K. Gui, M. Wang, Silicon carbide nanowire modified mullite fabric hierarchical structure applied as a stable and self-cleaning superhydrophobic material, Mater. Des. 210 (2021) 110044.

[42] M. Al-Fori, S. Dobretsov, M.T.Z. Myint, J. Dutta, Antifouling properties of zinc oxide nanorod coatings, Biofouling J. Bioadhesion Biofilm Res. 30 (7) (2014) 871-882.

[43] S. Jiang, T. Sreethawong, S.S.C. Lee, M.B.J. Low, K.Y. Win, A.M. Brzozowska, S. L-M. Teo, G.J. Vancso, D. Jan´czewski, M-Y. Han, Fabrication of copper nanowire films and their incorporation into polymer matrices for antibacterial and marine antifouling applications, Adv. Mater. Interfaces 2 (3) (2015) 1400483.

[44] M.S. Selim, H. Yang, S.A. El-Safty, N.A. Fatthallah, M.A. Shenashen, F.Q. Wang, Y. Huang, Superhydrophobic coating of silicone/β–MnO_2 nanorod composite for marine antifouling, Colloid. Surf. A Physicochem. Engin. Asp. 570 (2019) 518-530.

[45] (a) M. Ma, Y. Mao, M. Gupta, K.K. Gleason, G.C. Rutledge, Superhydrophobic fabrics produced by electrospinning and chemical vapor deposition, Macromolecules 38 (23) (2005) 9742–9748; (b) W.S.Y. Wong, G.Y. Liu, N. Nasiri, C.L. Hao, Z.K. Wang, A. Tricoli, Omnidirectional self-assembly of transparent superoleophobic nanotextures, ACS Nano 11 (2017) 1, 587–596.

[46] H. Shivashankar, A.M. Kevin, S.B.S. Manohar, S.M. Kulkarni, Investigation on dielectric properties of PDMS based nanocomposites, Physica B: Conden. Matter. 602 (2021) 412357.

[47] L.R.C. Moraes, H. Ribeiro, E. Cargnin, R.J. E. Andrade, M.F. Naccache, Rheology of graphene oxide suspended in yield stress fluid, J. Non-Newtonian Fluid Mech. 286 (2020) 104426.

[48] S. Medhi, S. Chowdhury, N. Bhatt, D.K. Gupta, S. Rana, J.S. Sangwai, Analysis of high performing graphene oxide nanosheets based non-damaging drilling fluids through rheological measurements and CFD studies, Powder Technol. 377 (2021) 379-395.

[49] S. Shrivastava, P. Shrivastava, J. Ramasamy, World health organization releases global priority list of antibiotic-resistant bacteria to guide research, discovery, and development of new antibiotics, J. Med. Soc. 32 (1) (2018) 76-76.

[50] M.S. Selim, H. Yang, F.Q. Wang, N.A. Fatthallah, Y. Huang, S. Kuga, Silicone/ZnO nanorod composite coating as a marine antifouling surface, Appl. Surf. Sci. 466 (2019) 40-50.

[51] A.J. Chalk, J.F. Harrod, Homogeneous catalysis. II. The mechanism of the hydrosilation of olefins catalyzed by group VIII metal complexes, J. Am. Chem. Soc. 87 (1965) 16–21.

[52] (a) D. Owens, R. Wendt, Estimation of the surface free energy of polymers, J. Appl. Polym. Sci. 13 (1969) 1741–1747; (b) D.H. Kaelble, Dispersion-polar surface tension properties of organic solids, J. Adhesion 2 (1970) 66–81.

[53] S.K. Rath, J.G. Chavan, S. Sasane, Jagannath, M. Patri. Two component silicone modified epoxy foul release coatings: effect of modulus, surface energy and surface restructuring on pseudobarnacle and macrofouling behavior. Appl. Surf. Sci. 256 (2010) 2440–2446.

[54] EN ISO 6272-1, paints and varnishes-Rapid-Deformation (impact resistance) tests – Part1: Falling-Weight Test, Large-Area Indenter, CEN, Brussels, Belgium, 2002.

[55] ASTM-D3359-02, Standard Test Methods for measuring (ASTM) Adhesion by Tape Test, Philadelphia, PA, USA, 2002.

[56] ASTM D522, Standard Method for Manderal Bend Test of Attached Organic Coatings,

American Society for Testing and Materials, Philadelphia, 1988.

[57] F. Traon, K. Réhel, I. Linossier, F. Faÿ. Potential antifouling properties of copper loaded zeolites on fouling diatoms, Microporous Mesoporous Mater. 312 (2021) 110734.

[58] Y. Duan, J. Wu, W. Qi, R. Su. Eco-friendly marine antifouling coating consisting of cellulose nanocrystals with bioinspired micromorphology, Carbohydr. Polym. 304 (2023) 120504.

[59] M.S. Selim, A. Elmarakbi, A.M. Azzam, M.A. Shenashena, A.M. EL-Saeed, Sherif A. El-Safty. Eco-friendly design of superhydrophobic nano-magnetite/silicone composites for marine foul-release paints, Prog. Org. Coat. 116 (2018) 21–34.

[60] A.M. Azzam, M.A. Shenashen, B.B. Mostafa, W.A. Kandeel, S.A. El-Safty. Antibacterial activity of magnesium oxide nanohexagonal sheets for wastewater remediation, Environ. Prog. Sustain. Energy 38 (S1) (2019) 260-266.

[61] N. Niboucha, C. Goetz, L. Sanschagrin, J. Fontenille, I. Fliss, S. Labrie, J. Jean, Comparative study of different sampling methods of biofilm formed on stainless-steel surfaces in a CDC biofilm reactor, Front. Microbiol. 13 (2022) 892181.

[62] A.A. Askar, M.S. Selim, S.A. El-Safty, A.I. Hashem, M.M. Selim, M.A. Shenashen, Antimicrobial and immunomodulatory potential of nanoscale hierarchical one-dimensional zinc oxide and silicon carbide materials, Mater. Chem. Phys. 263 (2021) 124376.

[63] M.S. Selim, Z. Hao, P. Mo, J. Yi, H. Ou, Biobased alkyd/graphene oxide decorated with β–MnO_2 nanorods as a robust ternary nanocomposite for surface coating, Colloid Surf. A: Physicochem. Engin. Asp. 601 (2020) 125057.

[64] M.S. Selim, H. Yang, F.Q. Wang, N.A. Fatthallah, X. Li, Y. Li, Y. Huang, Superhydrophobic silicone/SiC nanowire composite as a fouling release coating material, J. Coat. Technol. Res. 16 (2019) 1165–1180.

[65] J-P. Chen, Z-F. Wang, Z-L. Yi, L-J. Xie, Z. Liu, S-C. Zhang, C-M. Chen, SiC whiskers nucleated on rGO and its potential role in thermal conductivity and electronic insulation, Chem. Engin. J. 423 (2021) 130181.

[66] Z. Dong, J. Meng, H. Zhu, G. Yuan, Y. Cong, J. Zhang, X. Li, A. Westwood, Synthesis of SiC nanowires via catalyst-free pyrolysis of silicon-containing carbon materials derived from a hybrid precursor, Ceram. Int. 43 (2017) 11006–11014.

[67] R. Qian, J. Yu, C. Wu, X. Zhai, P. Jiang, Alumina-coated graphene sheet hybrids for electrically insulating polymer composites with high thermal conductivity, RSC Adv. 3 (2013) 17373–17379.

[68] J. Song, Y. Zhang, Vertically aligned silicon carbide nanowires/reduced graphene oxide networks for enhancing the thermal conductivity of silicone rubber composites, Compos. Part A Appl. Sci. Manuf. 133 (2020) 105873.

[69] N. Song, D. Jiao, P. Ding, S. Cui, S. Tang, L. Shi, Anisotropic thermally conductive flexible films based on nanofibrillated cellulose and aligned graphene nanosheets, J. Mater. Chem. C 4 (2016) 305–314.

[70] M. Khan, M.N. Tahir, S.F. Adil, H.U. Khan, M.R.H. Siddiqui, A.A. Al-warthan, W. Tremel, Graphene based metal and metal oxide nanocomposites: synthesis, properties and their applications, J. Mater. Chem. A. 3 (2015) 18753–18808.

[71] A. Kaffashi, A. Jannesari, Z. Ranjbar. Silicone fouling-release coatings: effects of the molecular weight of poly(dimethylsiloxane) and tetraethyl orthosilicate on the magnitude of pseudobarnacle adhesion strength, Biofoul. 28 (7) (2012) 729-41.

[72] M.Z. Rong, M.Q. Zhang, W.H. Ruan. Surface modification of nanoscale fillers for improving properties of polymer nanocomposites: A review, Mater. Sci. Technol. 22 (2006) 787–797.

[73] A. Razmjoua, J. Mansouri, V. Chen, The effects of mechanical and chemical modification of TiO_2 nanoparticles on the surface chemistry, structure and fouling performance of PES ultrafiltration membranes, J. Membr. Sci. 378 (2011) 73–84.

[74] B. Cortese, S. D'Amone, M. Manca, I. Viola, R. Cingolani, G. Gigli, Superhydrophobicity due to the hierarchical scale roughness of PDMS surfaces, Langmuir 24 (2008) 2712–2718.

[75] S. Barthwal, S. Barthwal, B. Singh, N. Bahadur Singh, Multifunctional and fluorine-free

superhydrophobic composite coating based on PDMS modified MWCNTs/ZnO with self-cleaning, oil-water separation, and flame retardant properties, Colloid. Surf. A: Physicochem. Engin. Asp. 597 (2020) 124776.

[76] Y. Deng, D. Mager, Y. Bai, T. Zhou, Z. Liu, L. Wen, Y. Wu, J.G. Korvink, Inversely designed micro-textures for robust Cassie-Baxter mode of superhydrophobicity, Comput. Methods Appl. Mech. Eng. 341 (2018) 113–132.

[77] T. Sun, L. Feng, X. Gao, L. Jiang, Bioinspired surfaces with special wettability, Acc. Chem. Res. 38 (8) (2005) 644–652.

[78] N.V. Motlagh, R. Khani, S. Rahnama, Super dewetting surfaces: focusing on their design and fabrication methods, Colloids Surf. A Physicochem. Eng. Asp. 484 (2015) 528–546.

[79] M.S. Selim, F.Q. Wang, H. Yang, Y. Huang, S. Kuga, Hyperbranched alkyd/magnetite-silica nanocomposite as a coating material, Mater. Des. 135 (2017) 173–183.

[80] K. Bruellhoff, J. Fiedler, M. MöLler, J. Groll, R.E. Brenner, Surface coating strategies to prevent biofilm formation on implant surfaces, Int. J. Artif. Organs. 33 (2010) 646−653.

[81] E. Richard, S.T. Aruna, B.J. Basu, Superhydrophobic surfaces fabricated by surface modification of alumina particles. App. Surf. Sci. 258 (2012) 10199−10204.

List of Figures and Scheme:

Figure 10. Bacterial biofilm's fluorescence microscopic captures for (A) unfilled PDMS, (B) 0.25 wt.%, (C) 0.5 wt.%, (D) 1 wt.%, (E) 2 wt.%, and (F) 3 wt.% concentrations of RGO/β-SiC nanocomposite specimens incubation for 4 weeks.

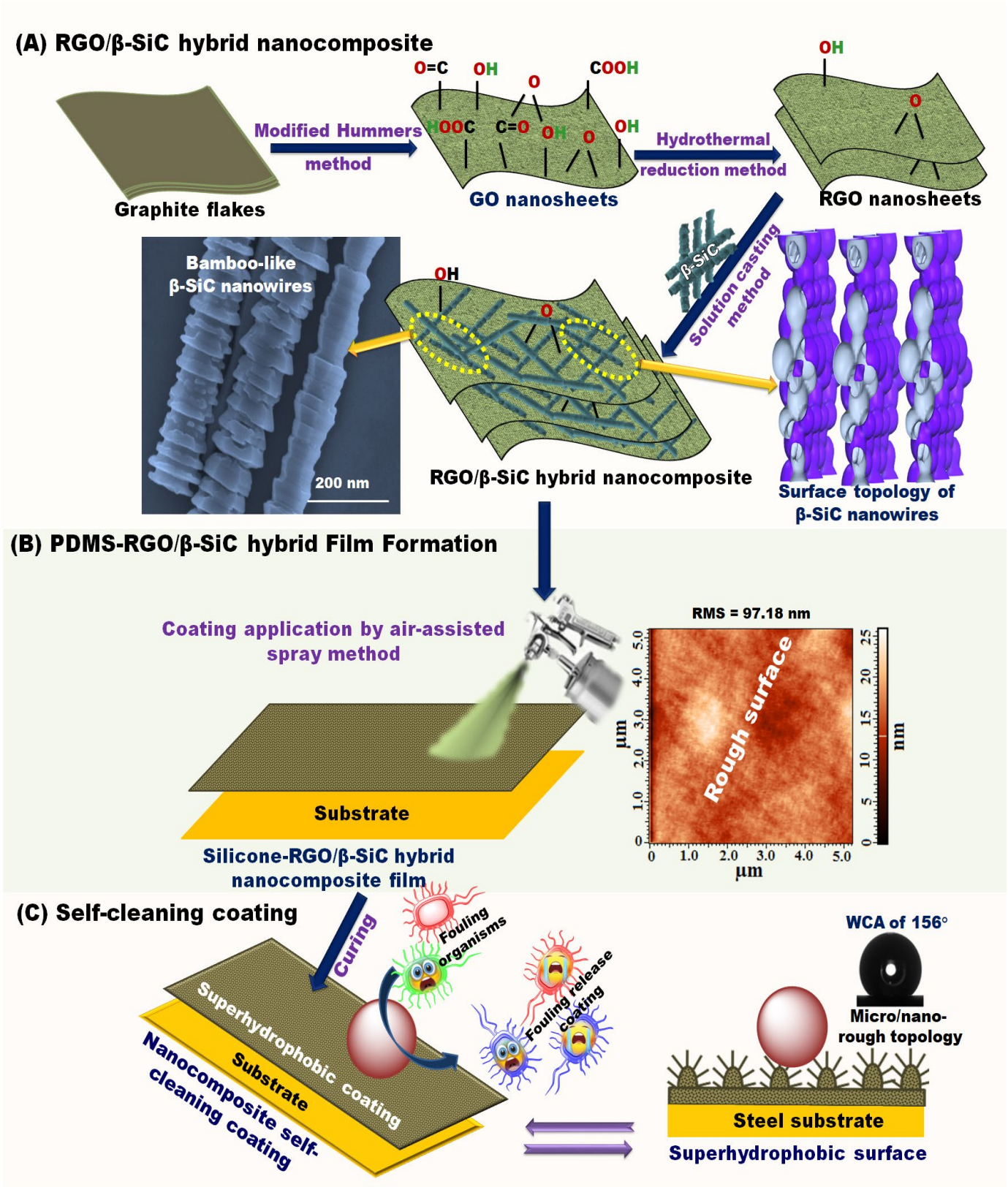
(A) RGO/β-SiC hybrid nanocomposite
Graphite flakes
Modified Hummers method
GO nanosheets
Hydrothermal reduction method
RGO nanosheets
Bamboo-like β-SiC nanowires
200 nm
β-SiC
Solution casting method
RGO/β-SiC hybrid nanocomposite
Surface topology of β-SiC nanowires
(B) PDMS-RGO/β-SiC hybrid Film Formation
Coating application by air-assisted spray method
Substrate
Silicone-RGO/β-SiC hybrid nanocomposite film
RMS = 97.18 nm
Rough surface
μm
nm
(C) Self-cleaning coating
Curing
Fouling organisms
Superhydrophobic coating
Substrate
Nanocomposite self-cleaning coating
Fouling release coating
WCA of 156°
Micro/nano-rough topology
Steel substrate
Superhydrophobic surface

Scheme 1.

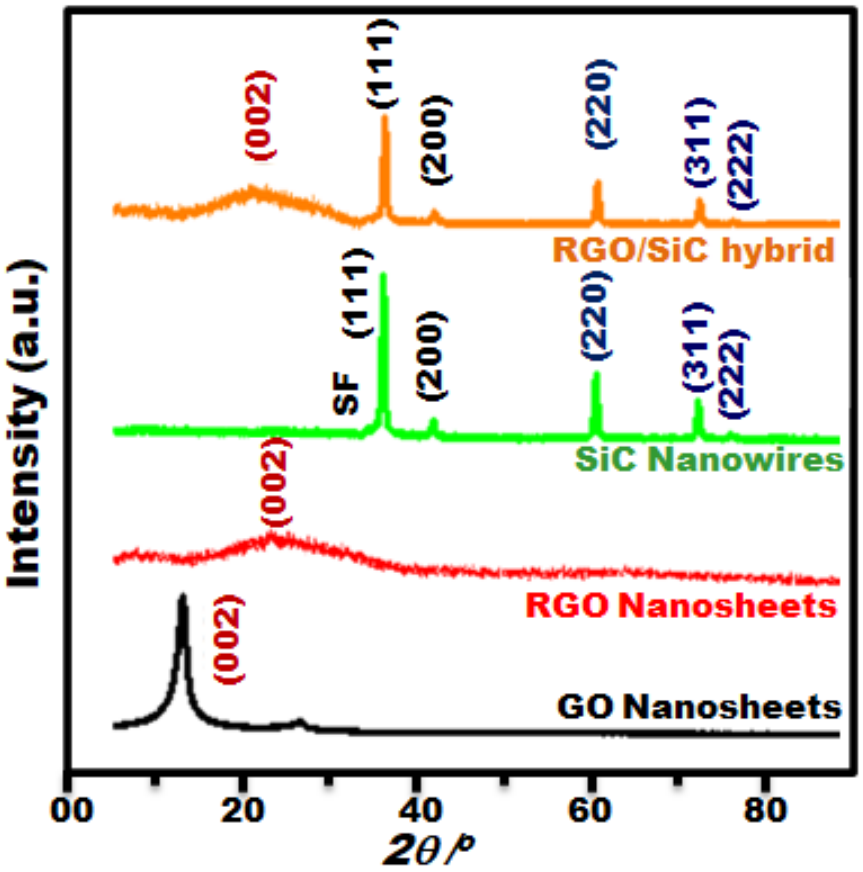
Intensity (a.u.)
(002)
(111)
(200)
(220)
(311)
(222)
RGO/SiC hybrid
SF
(111)
(200)
(220)
(311)
(222)
SiC Nanowires
(002)
RGO Nanosheets
(002)
GO Nanosheets
00
20
40
60
80
2θ/°

Figure 1.

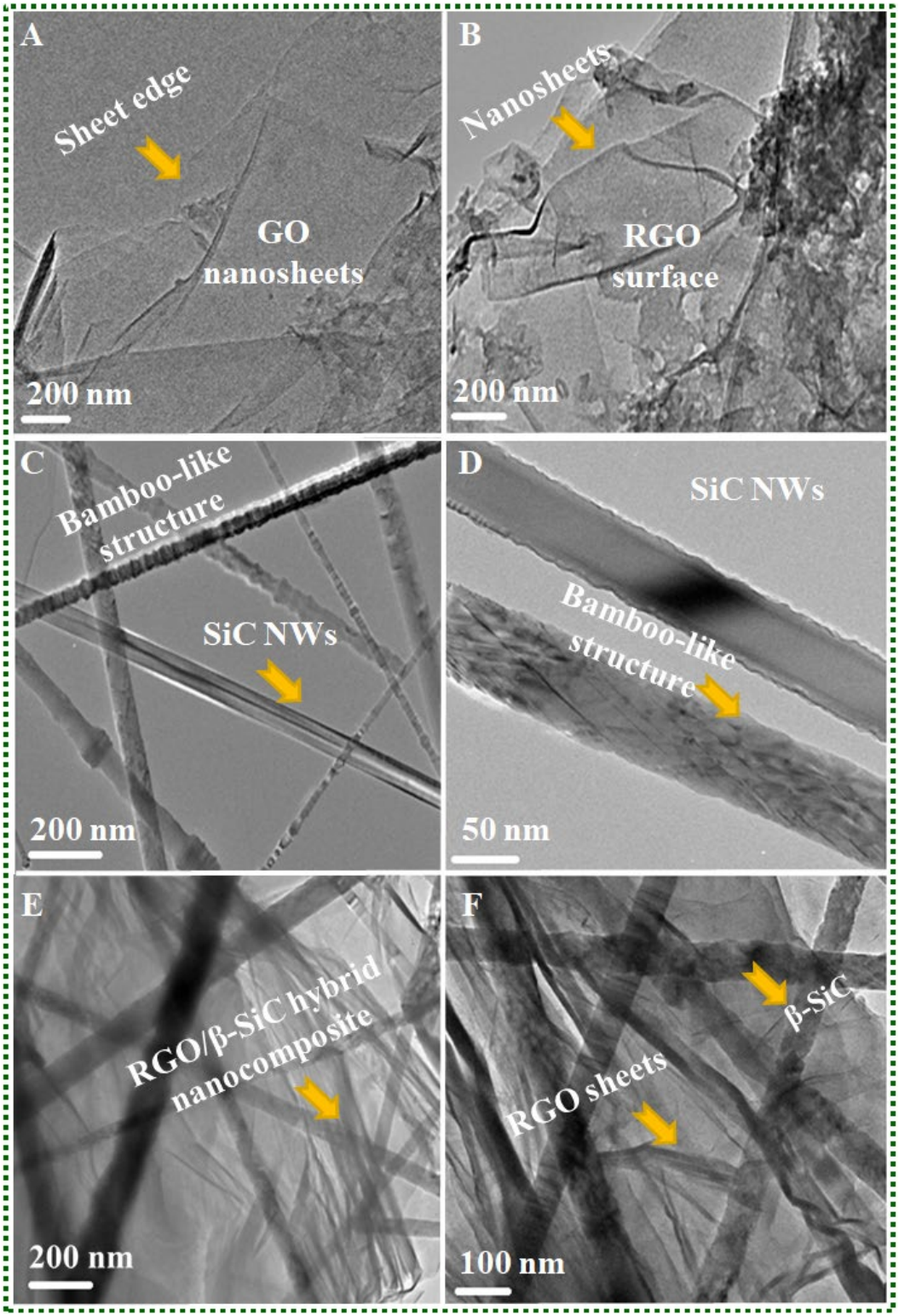
A
Sheet edge
GO
nanosheets
200 nm
B
Nanosheets
RGO
surface
200 nm
C
Bamboo-like
structure
SiC NWs
200 nm
D
SiC NWs
Bamboo-like
structure
50 nm
E
RGO/β-SiC hybrid
nanocomposite
200 nm
F
β-SiC
RGO sheets
100 nm

Figure 2.

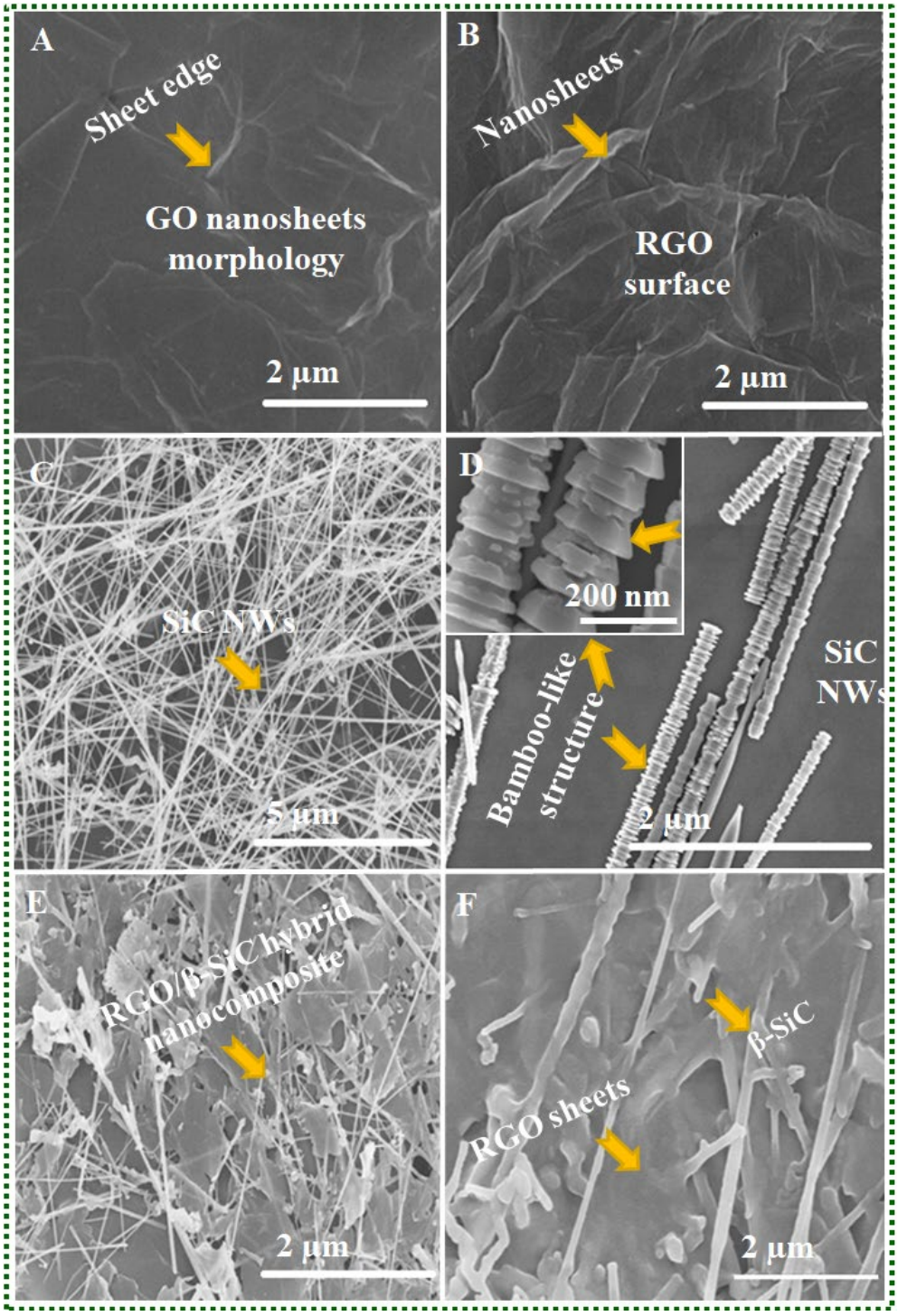
A
Sheet edge
GO nanosheets morphology
2 μm
B
Nanosheets
RGO surface
2 μm
C
SiC NWs
5 μm
D
200 nm
Bamboo-like structure
SiC NWs
2 μm
E
RGO/β-SiC hybrid nanocomposite
2 μm
F
β-SiC
RGO sheets
2 μm

Figure 3.

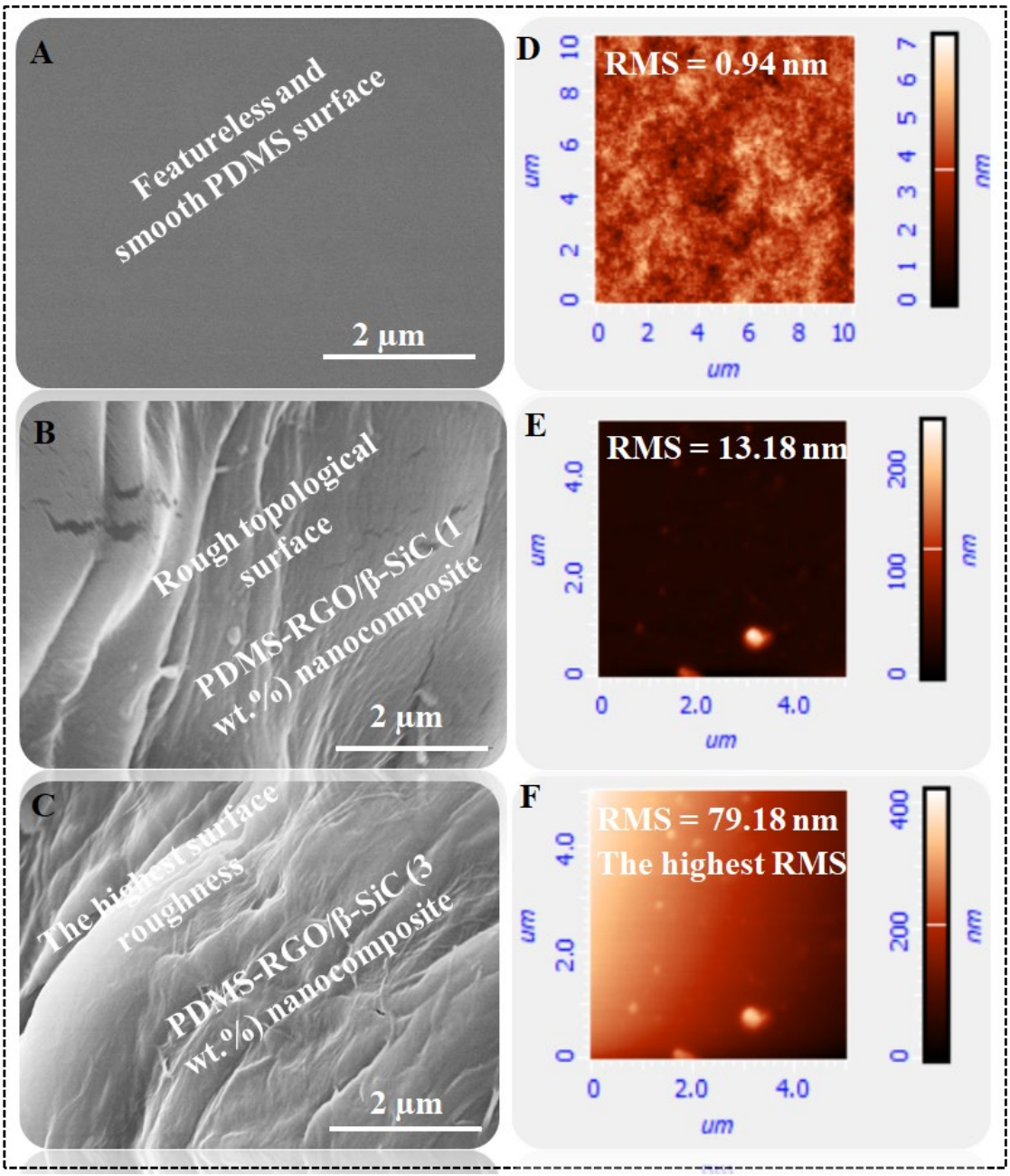
A
Featureless and smooth PDMS surface
2 µm
D
RMS = 0.94 nm
um
nm
B
Rough topological surface
PDMS-RGO/β-SiC (1 wt.%) nanocomposite
2 µm
E
RMS = 13.18 nm
um
nm
C
The highest surface roughness
PDMS-RGO/β-SiC (3 wt.%) nanocomposite
2 µm
F
RMS = 79.18 nm
The highest RMS
um
nm

Figure 4.

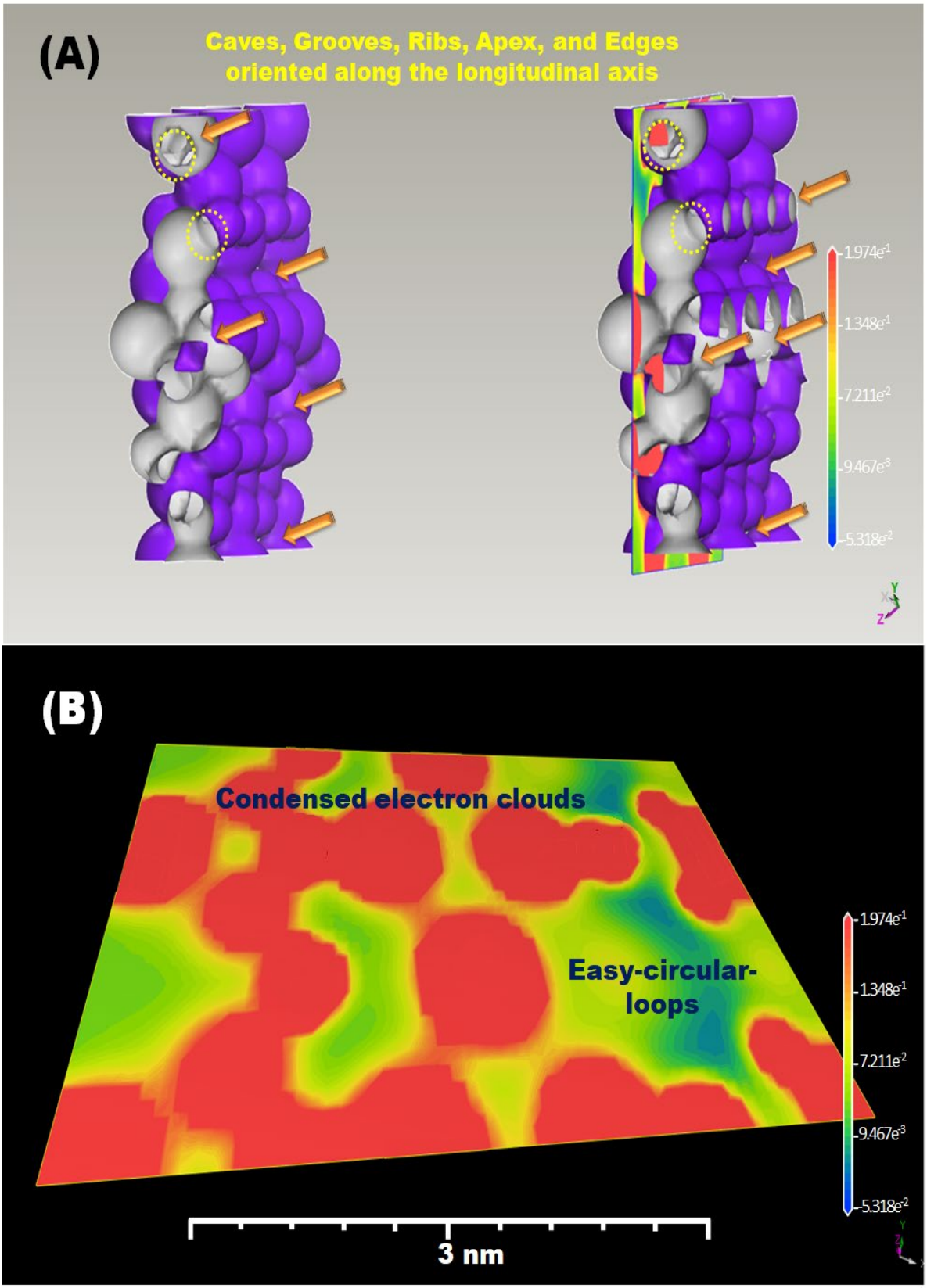
(A)
Caves, Grooves, Ribs, Apex, and Edges
oriented along the longitudinal axis
1.974e-1
1.348e-1
7.211e-2
9.467e-3
5.318e-2
(B)
Condensed electron clouds
Easy-circular-loops
3 nm

Figure 5.

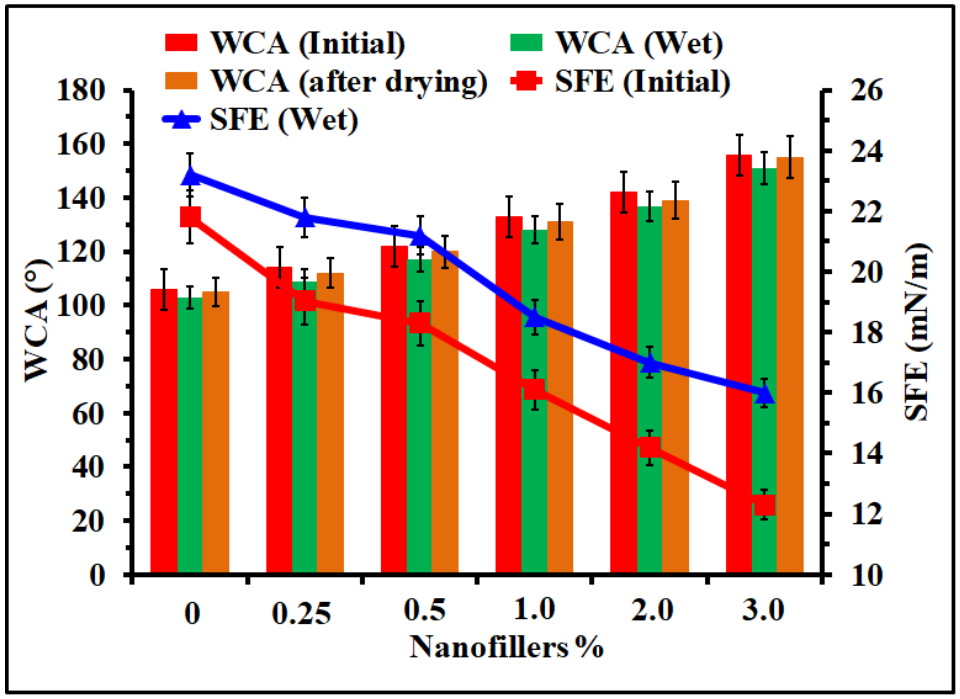

Figure 6.

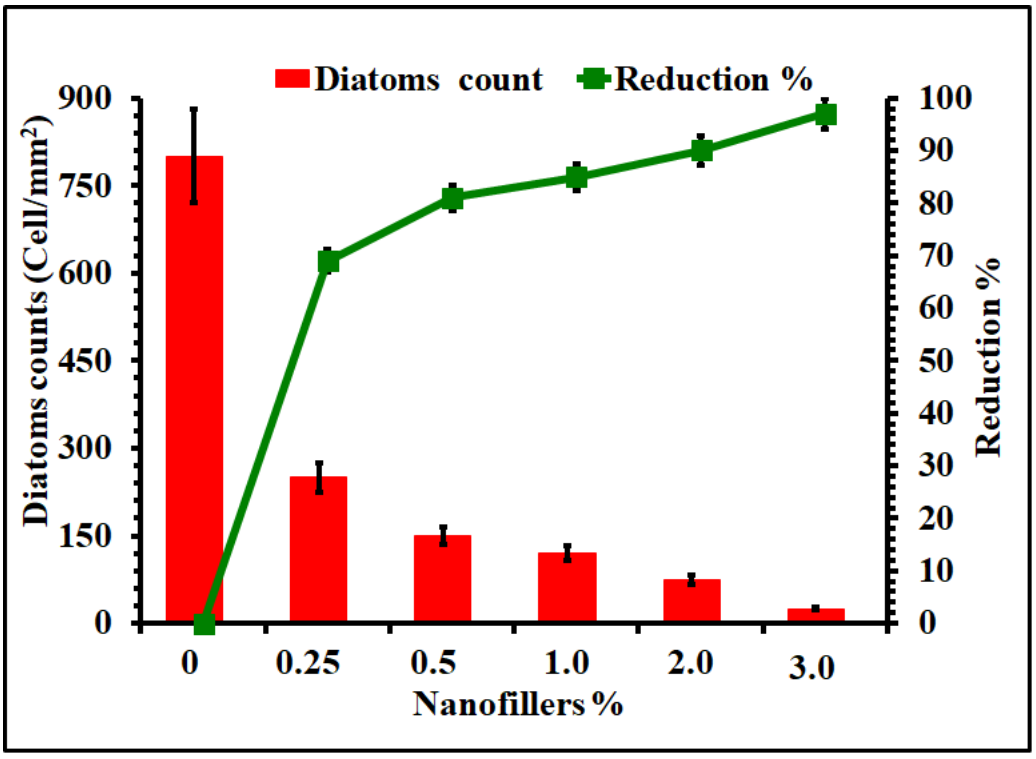

Figure 7.

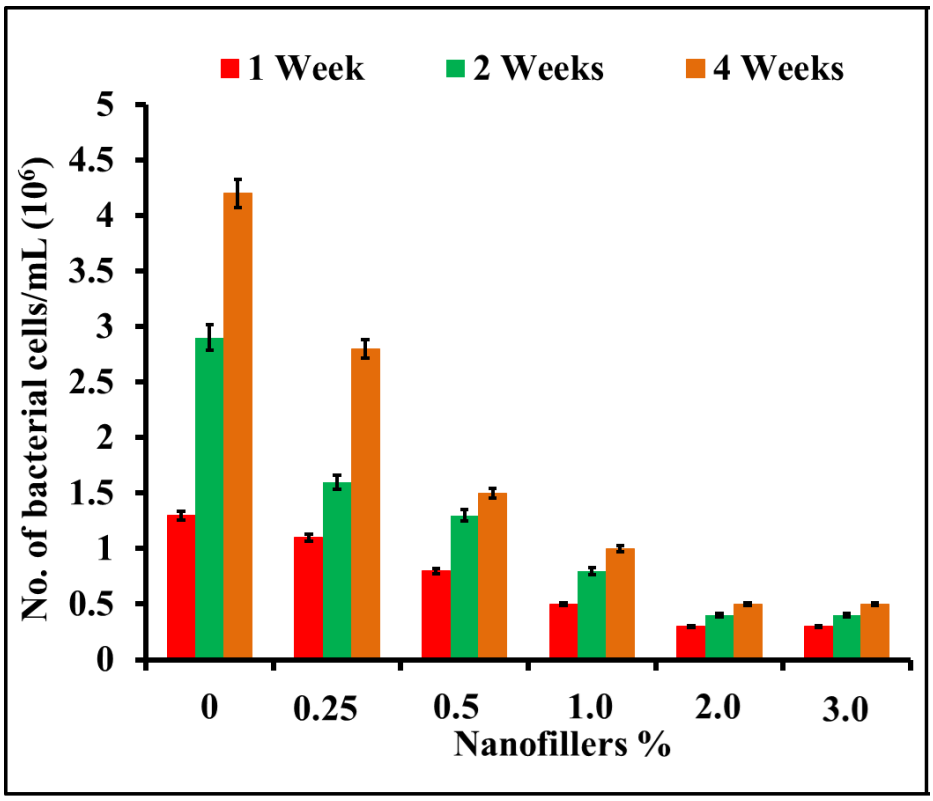
1 Week
2 Weeks
4 Weeks
No. of bacterial cells/mL (10^6)
5
4.5
4
3.5
3
2.5
2
1.5
1
0.5
0
0
0.25
0.5
1.0
2.0
3.0
Nanofillers %

Figure 8.

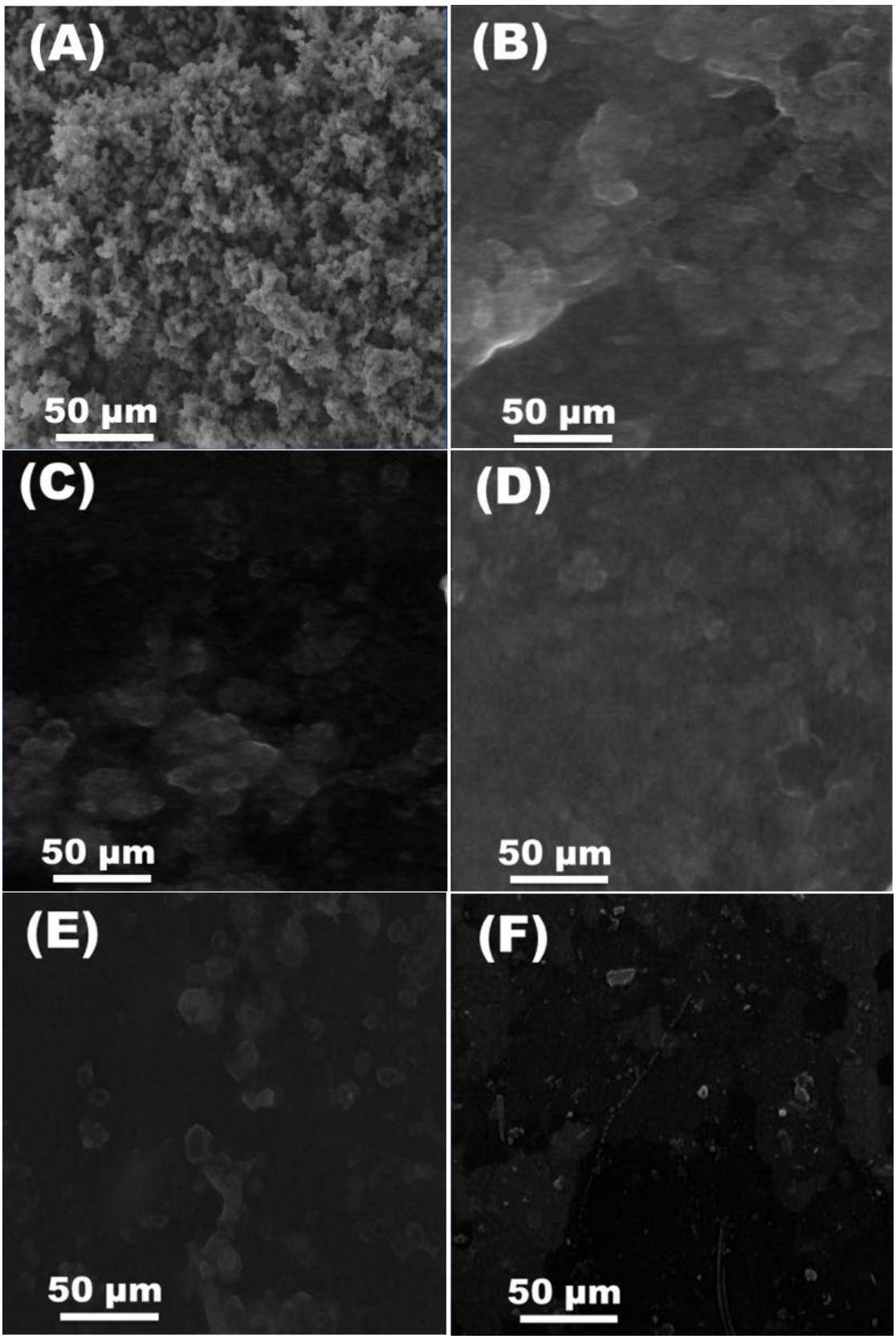

Figure 9.

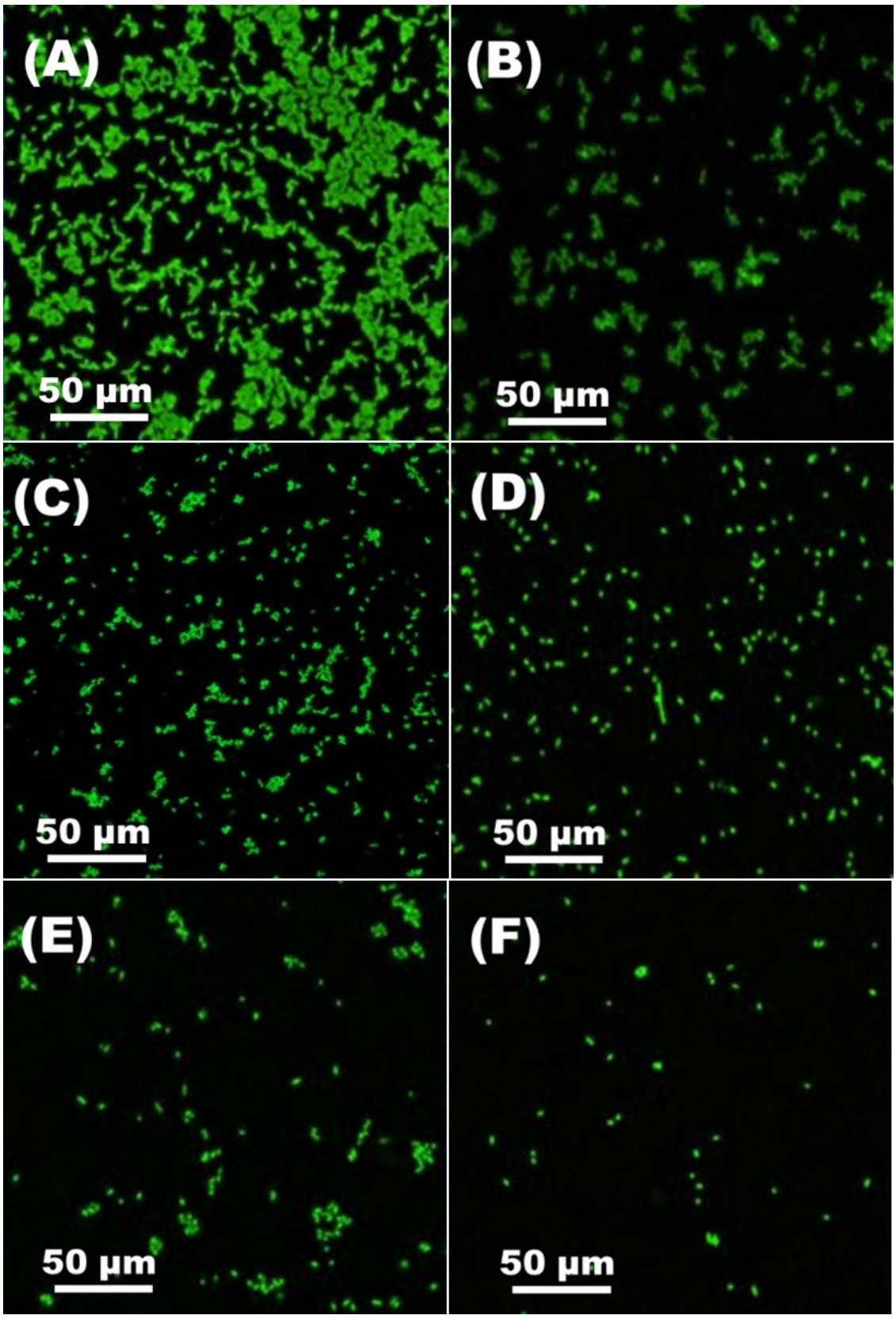

Figure 10.

List Of Tables:

Table 1. The results of the mechanical tests for PDMS-RGO/β-SiC nanocomposite coatings.

Properties	Concentration of RGO/β-SiC nanofiller in PDMS surfaces					
	0.0 wt.%	**0.25 wt.%**	**0.5 wt.%**	**1 wt.%**	**2 wt.%**	**3 wt.%**
Impact resistance (joule)	6	8	9	12	13	16
Cross-hatch	Pass	Pass	Pass	Pass	Pass	Pass
T-bending	< 5	< 5	< 5	< 5	< 5	< 5